

# Verification of the feasibility of higher-order modulation for long-range communication in deep water

## 심해 장거리 통신에서의 고차 변조 기법의 활용 가능성 검증

Donghyeon Kim,<sup>1</sup> J. S. Kim,<sup>2†</sup> and Joo Young Hahn<sup>3</sup>

(김동현,<sup>1</sup> 김재수,<sup>2†</sup> 한주영<sup>3</sup>)

<sup>1</sup>KIOST-KMOU OST School, <sup>2</sup>Korea Maritime and Ocean University, <sup>3</sup>Agency for Defense Development  
(Received July 6, 2021; revised August 6, 2021; accepted August 18, 2021)

**ABSTRACT:** For long-range communication in deep water, low carrier frequency is efficient due to a decrease in transmission loss. However, there is a limitation in that the data rate decreases due to a narrow bandwidth. In order to increase the data rate in an environment with a limited bandwidth, it is necessary to design a higher-order modulation scheme. This paper analyzes the long-range communication data modulated by higher-order modulation schemes. The long-range communication experiment (23 km ~) was conducted in East Sea in October 2020. During the experiment, a vertical line array was utilized and communication sequences were modulated by Phase Shift Keying (PSK) and Quadrature Amplitude Modulation (QAM) schemes and transmitted by a towed source. In more detail, PSK modulation consists of quadrature PSK and 8PSK, QAM modulation consists of 8QAM and 16QAM. Time reversal processing is applied to mitigate inter-symbol interference by utilizing the correlation between received signals and channel impulse responses. All modulation schemes show successful results at 23 km range, demonstrating the feasibility of higher-order modulation in long-range communication.

**Keywords:** Deep water, Long-range communication, Time reversal processing, Higher-order modulation

**PACS numbers:** 43.60.Dh, 43.60.Tj, 43.60.Fg

**초 록:** 심해 장거리 통신에서는 전달 손실이 적은 낮은 반송 주파수가 효율적이지만, 좁은 대역폭을 가지는 제약이 따른다. 대역폭의 감소는 전송률의 감소를 의미하며, 제한된 대역폭을 가진 환경에서 전송률을 증가시키기 위해서는 고차 변조 기법으로 설계될 필요가 있다. 본 논문은 고차 변조 기법으로 설계된 장거리 수중음향통신 데이터 분석 결과를 제시한다. 2020년 10월 동해에서 예인 음원을 이용한 장거리 해상실험 (23 km ~)이 수행되었고, 수직 선 배열을 통해 데이터를 획득하였다. 본 연구팀은 위상 변조 방식이 적용된 Phase Shift Keying (PSK) 계열 신호와 위상 및 진폭 변조 방식이 적용된 Quadrature Amplitude Modulation (QAM) 계열의 신호를 송신하였으며, 구체적으로 각 계열별 두 종류의 신호를 설계하였다; 1) PSK : quadrature PSK and 8PSK, 2) QAM : 8QAM and 16QAM. 데이터 분석을 위해 수신 신호와 채널 임펄스 응답 사이의 상관성을 활용하여 심볼 간 간섭을 완화시키는 시역전 처리가 적용되었다. 23 km 거리 데이터에 대해 모든 변조 방식이 성공적으로 복조됨으로써 장거리 환경에서 고차 변조 기법의 활용 가능성을 실험적으로 확인하였다.

**핵심용어:** 심해, 장거리 통신, 시역전 처리, 고차 변조 기법

## I. Introduction

In deep water long-range communication, the effect of

inter-symbol interference due to multipath is greater than in short-range communication, and the increase in transmission loss results in the use of lower carrier

†Corresponding author: J. S. Kim (jskim@kmou.ac.kr)

Department of Ocean Engineering, Korea Maritime and Ocean University, 727 Taejong-Ro, Yeongdo-Gu, Busan 49112, Republic of Korea

(Tel: 82-51-410-4325, Fax: 82-51-403-4320)



Copyright©2021 The Acoustical Society of Korea. This is an Open Access article distributed under the terms of the Creative Commons Attribution Non-Commercial License which permits unrestricted non-commercial use, distribution, and reproduction in any medium, provided the original work is properly cited.

frequencies for effective signal transmission. High carrier frequencies allow the use of wide bandwidths, which enable higher data rates,<sup>[1]</sup> whereas a low carrier frequency in a long-range environment has the constraint of a narrow bandwidth. A smaller bandwidth translates to reduced data rates. Kilfoyle outlined the specifications of underwater telemetry modems and presented the ‘range-rate product’, which is a metric for data rate reduction with an increasing range within 10 km.<sup>[2]</sup> Shimura added experimental results to improve and supplement the metric.<sup>[3]</sup>

As shown in References [1] and [2], while the data rate within 10 km is several tens of thousands of Bits Per Second (BPS), in the case of long-range deep-water communication, previous studies reported data rates of less than 1,000 bps.<sup>[4-23]</sup> Techniques such as higher-order modulation and multiple-input-multiple-output have been used to overcome the problem of low data rates overseas<sup>[4-6,11,13-16,18,19]</sup>, however, in Korea, only studies using Binary Phase-Shift Keying (BPSK), i.e., the lowest-order modulation scheme, have been reported.<sup>[20-23]</sup>

In this study, we investigated higher-order modulation schemes for long-range communication with the aim of improving the data rate. Data from Application-Adaptive Covert Underwater Acomm. EXperiment 2020 (ACUA-EX20) was obtained in the East Sea in October 2020. During the at-sea experiment, two types of PSK modulation signals and two types of Quadrature Amplitude Modulation (QAM) signals, which are higher-order modulations, were designed. A Vertical Line Array (VLA) was used for data acquisition, and the data were analyzed using time reversal communication, a method widely used in long-range environments for deriving an optimal solution by exploiting the reciprocity of the channel and combining it with a single channel equalizer.<sup>[7-10,12,16,17,19,21-26]</sup>

The remainder of this paper is organized as follows. Section II introduces ACUA-EX20, an at-sea experiment referred to in this paper, and the transmitted signals designed using higher-order modulation. In Sec. III, for at-sea environmental analysis, the Signal to Noise Ratio (SNR) is calculated, and the Doppler effect and channel

impulse response are estimated. Section IV presents the performance of the analysis of communication along with examples of signal reconstruction using time reversal processing; the results are also compared in terms of data rates with values reported in overseas research. Finally, Sec. V concludes the paper.

## II. ACUA-EX20

### 2.1 At-sea experiment design

In October 2020, ACUA-EX20, a long-range underwater acoustic communication experiment hosted by the Agency for Defense Development (ADD) with participation from several universities, was conducted in the east of Pohang. The purpose of our study was to analyze the performance of communication based on higher-order modulation to improve the data rate in long-range environments. Fig. 1 shows the experiment site where the experiment was conducted, and the yellow and red circles indicate the locations of the source and VLA, respectively. The source was connected to the Research Vessel (R/V) Cheonghae owned by the ADD and towed at the speed of 3 kn in the east direction.

Fig. 2 presents a schematic of the at-sea experiment, and expressing the sound speed profile, depth of the source and VLA, and seafloor topography. In the long-range experiment, the transmission loss was significantly increased, and the extent of the transmission loss varied with respect to the acoustic axis depth, source depth, and range. An increase in the transmission loss indicates a decrease in the SNR, which is represented as a widened area of the

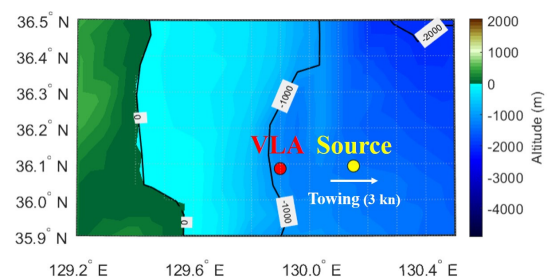


Fig. 1. (Color available online) Experimental site.

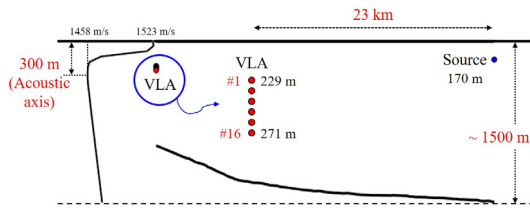


Fig. 2. (Color available online) Schematic of ACUA-EX20.

estimated symbols in terms of constellation in communication. More specifically, high-order modulation, in which the inter-symbol distance on the constellation (Euclidean distance) is reduced, has limitations in long-range experiments. Therefore, to minimize the transmission loss, the signals are transmitted using a Deep Sound Channel (DSC). To utilize the DSC, first, the acoustic axis depth should be evaluated by measuring the sound speed profile. As shown in Fig. 2, the acoustic axis formed around the depth at 300 m in the sound speed profile measured at the source position. Specifically, it is more effective to maintain the depth of the source as close to 300 m as possible. However, the depth of the source was limited owing to factors such as the maximum cable length, rise of the source during towing, and weather conditions. Therefore, in this experiment, the depth was maintained at 170 m during towing.

In the deep water of the East Sea, the sound speed profile shows a more rapid change toward the sea surface direction than to the seafloor direction relative to the acoustic axis, and the shadow zone becomes wider owing to the source located 130 m above the depth of the acoustic axis. Accordingly, the convergence zone was checked to set the range for signal transmission. Fig. 3(a) shows the results of transmission loss in the ACUA-EX20 environment calculated using the underwater sound propagation model. In the area with the depth of 229 m – 271 m where the VLA is installed, a zone with considerably low transmission loss (approximately 3 km – 18 km) close to the shadow zone was confirmed, and it can be observed that from 18 km or above, the area corresponds to the convergence zone apart from some sections. In this way, we transmitted communication signals in the vicinity of 23

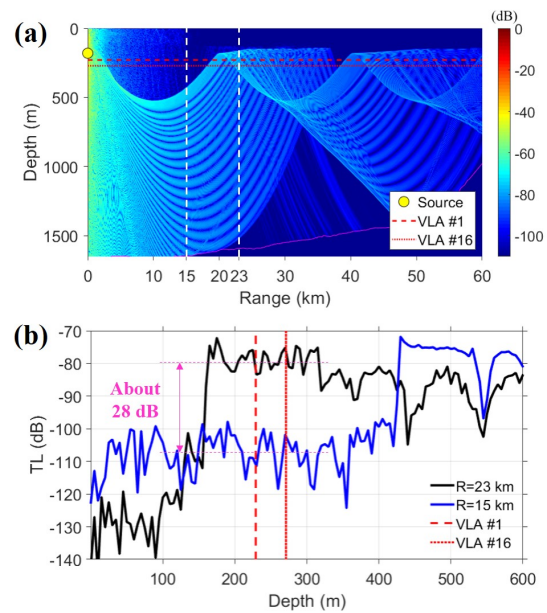


Fig. 3. (Color available online) (a) Transmission loss at 2,560 Hz for a source at 170-m depth. (b) Transmission loss as a function of depth at 15 and 23 km, indicated as white dashed lines in (a).

km, which is a part of the convergence zone. To evaluate in detail the difference in transmission loss between the convergence zone and the other regions, Fig. 3(b) shows the results of transmission loss per depth at two ranges: 15 km, which is one of the sections with low transmission loss, and 23 km, which is the range at which the signal is transmitted, as indicated by the white dashed lines in Fig. 3(a). It can be observed that the transmission loss in the range of 23 km from the depth where the VLA is located is, on average, approximately 28 dB lower than the transmission loss at 15 km. The result indicates that in a long-range environment with a large transmission loss, signal transmission using the convergence zone is relatively effective in DSC.

## 2.2 Design of transmitted signal packet

Fig. 4 shows the configuration of the transmitted signal packets to be analyzed in this study. The transmitted signal comprises a probe signal with the duration of 0.5 s for estimation of channel impulse response, guard time with the duration of 0.5 s, and a communication signal with the

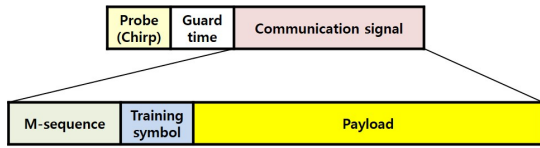


Fig. 4. (Color available online) Structure of the transmitted signal packet.

duration of 2.95 s. In the waveguide, when towing a source, the longer the duration of the signal, the more likely the Doppler shift occurs with time in the signal. Therefore, a communication signal is designed to minimize the duration. After designing the probe signals as chirp signals, a Hanning window was applied, and the carrier frequency and bandwidth were 2,560 and 1,024 Hz, respectively. The communication signals were designed using a Root-Raised Cosine (RRC) filter with the roll-off factor of 0.5 with a data rate of approximately 683 sps, comprising an M-sequence signal, 200 training symbols, and 1,300 payloads. The M-sequence signal is designed for Doppler estimation and synchronization and consists of 511 symbols to improve the estimation accuracy of synchronization of the received signals in a long-range environment where transmission loss is significantly increased. In addition, the configuration of the M-sequence signal of the duration is effective for Doppler estimation in a towing situation. Two hundred training symbols were designed for the equalizer application after time reversal processing. The RRC filter is used as a matched filter in the modulation/demodulation process. The frequency band of the communication signals is similar to that of the probe signals.

As described above, compared with short-range propagation, in long-range propagation, the available frequency bandwidth owing to transmission loss is reduced. Specifically, as the transmission range increases, the design data rate decreases. To increase the data rate in such environments with limitations, the use of a high-order modulation scheme may be an effective strategy. We designed the training symbols and payloads as Quadrature Phase Shift Keying (QPSK), 8PSK, 8QAM, and 16QAM, the higher-order modulation, and each signal was transmitted

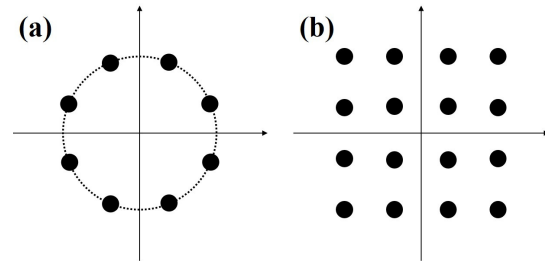


Fig. 5. Scatter plots of higher-order modulation transmitted during ACUA-EX20: (a) 8PSK, the highest order modulation of PSK modulation; (b) 16QAM, the highest order modulation of QAM.

four times. PSK is a phase modulation technique, and QAM utilizes both phase and amplitude modulation. Because QAM uses amplitude modulation, it is sensitive to noise. Among them, the 16QAM signal is the most challenging owing to its short Euclidean distance. The spectral efficiency of the signals designed in this study ranges from a minimum of 1.33 bits/s · Hz (QPSK) to the maximum of 2.67 bits/s · Hz (16QAM). In Figs. 5(a) and 4(b), the constellations for the highest order modulation schemes (8PSK and 16QAM) among the PSK and QAM designed during the experiment are presented as an example for each type of signal.

### III. At-sea environmental analysis

#### 3.1 Signal to Noise Ratio

The higher the SNR, the greater the probability of demodulation of the communication signals; thus SNR was first examined from the measured data. Fig. 6(a) shows the signals received during the experiment. As a visual example, one QPSK-modulated signal is illustrated out of multiple data packets. In Fig. 6(a), the blue and red lines are zones for calculating the signal and noise levels, respectively, and the SNR for each channel calculated from the two zones is shown in Fig. 6(b). The SNR for each channel is represented as error bars using the mean and variance values for all transmitted data packets (16 in total). In the fourth channel from the top (hereafter,

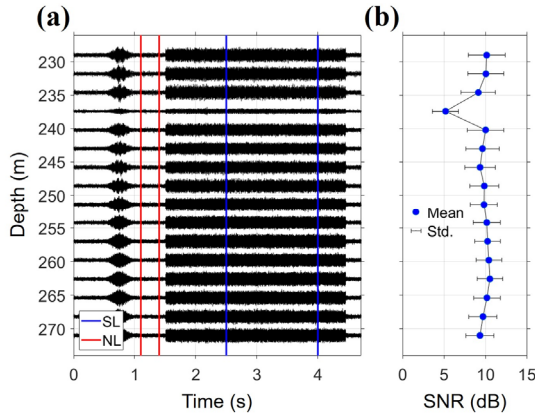


Fig. 6. (Color available online) SNRs of the received signals: (a) Waterfall plot of 5-s data received on the vertical line array; (b) SNRs as a function of the receiver depth.

channel 4), amplification was not performed properly inside the receiver, therefore, the SNR was lower than in other channels. Excluding channel 4, the SNR was 10 dB on average, and the strong intensity of incoming signals was numerically confirmed. Specifically, from the values, the successful demodulation of the signals can be predicted in advance.

### 3.2 Ambiguity function–based Doppler estimation

As described above, the source was towed during the experiment, and thus the received signals reflecting the Doppler effect were measured. Owing to the Doppler effect, the phase of the symbols is shown in a rotating form on the constellation; therefore, the Doppler effect have to be compensated before performing the communication performance analysis based on time reversal processing. Eq. (1) calculates the ambiguity function for Doppler estimation and shows matched filtering of the transmitted signal to the received signal,<sup>[27]</sup>

$$|\chi(t_r, \Delta f_d)|^2 = \left| \int_{-\infty}^{\infty} s(t) s^*(t+t_r) e^{i2\pi \Delta f_d t} dt \right|^2, (1)$$

Here  $s(t)$  denotes the transmitted signal, and  $s(t+t_r)$  denotes the signal including the time delay  $t_r$  of the

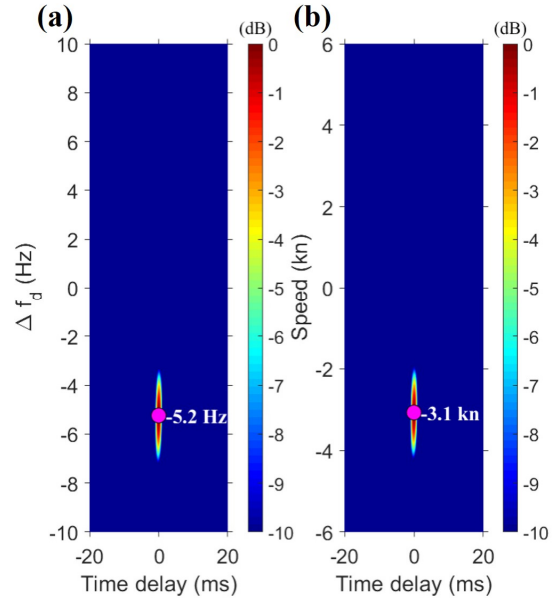


Fig. 7. (Color available online) Ambiguity function in terms of (a) Doppler frequency shift and (b) source (R/V) speed.

transmitted signal, i.e., the received signal;  $\Delta f_d$  represents the Doppler frequency shift with respect to the carrier frequency.

Fig. 7 shows the result of the ambiguity function calculated by applying the M-sequence signal instead of the transmitted signal in Eq. (1). The ambiguity functions are presented in Fig. 7(a) and 7(b) with respect to the Doppler frequency shift and the speed of the source connected to the R/V Cheonghae. The relationship between the Doppler frequency and speed of the source can be expressed as Eq. (2), and Fig. 7(b) is the representation of Fig. 7(a) in terms of the source speed using Eq. (2),

$$f_d = \left( \frac{1}{1 - v_s/c} \right) f_c \approx (1 + v_s/c) f_c = f_c + \Delta f_d. (2)$$

The second term of Eq. (2) represents the Doppler frequency regarding source movement, and when the source approaches from the receiver, the sign of the source speed,  $v_s$  is positive. Here,  $c$  indicates the speed of sound, and in general, because the source speed is small compared to the sound speed, it can be approximated to the third term by a geometric series. In the approximation equation, the

part except the carrier frequency can be expressed as a Doppler frequency shift, and the ambiguity function can be expressed from two aspects through the relationship between the Doppler frequency shift and the source speed.

The towing speed can be derived from the maximum value of the ambiguity function in terms of the source speed. As the source moved away from the receiver during the experiment, the line of sight was constant, and it can be predicted that the source speed and the estimated Doppler speed are similar. The maximum value in Fig. 7(b) can be observed at -3.1 kn. Because this value is almost the same as the towing speed 3kn in magnitude, and the source is towed away from the receiver in the negative direction, it can be observed that the Doppler estimation using the ambiguity function yields a reasonable result.

### 3.3 Channel impulse response

In this section, the channel impulse response is estimated using the probe signals. The channel impulse response can be estimated by applying the signals shown on the left side of Fig. 6(a) and the received probe signals to the matched filter, while Fig. 8 shows the channel impulse response result as a function of the depth. Information on delay spread can be obtained from the channel impulse response, and the generation of multipaths with a maximum length of 30 symbol lengths can be confirmed in the ACUA-EX20 environment. Converting this to time, this symbol

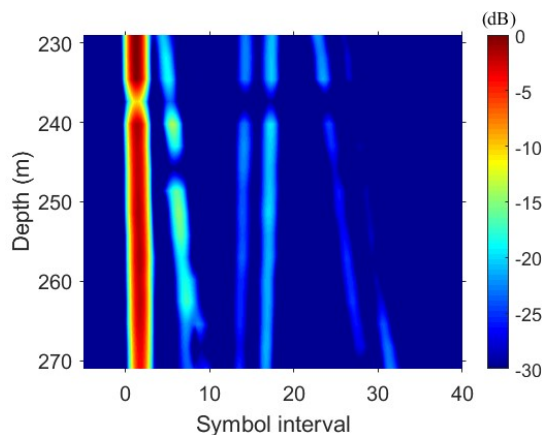


Fig. 8. (Color available online) Channel impulse response as a function of the symbol interval and depth.

length corresponds to approximately 0.05 s. The channel impulse response can also be regarded as the distribution of the arrival time of the eigenray between the source and receiver, as shown in Fig. 8, where the eigenray between the source and receiver varies according to the change in the receiver depth. This is effective with respect to the time reversal processing that exploits the diversity of channels, and this will be discussed in detail in the next section.

## IV. Communication performance analysis based on time reversal processing

### 4.1 Signal reconstruction using probe signal

Song proposed the  $q$ -function,  $q(t)$ , as a metric to analyze the performance of time reversal processing.<sup>[28]</sup>  $q(t)$  is defined as the sum of auto-correlation of all channels and can be expressed as Eq. (3),

$$q(t) = \sum_{i=1}^N h_i(-t) * h_i(t), \quad (3)$$

Here  $h_i(t)$  denotes the channel impulse response of the  $i$ th channel and  $N$  denotes the number of channels.

The closer the result of  $q(t)$  to the delta function, the better the performance of time reversal processing, indicating that the transmitted signals are well reconstructed. Fig. 9 shows the result of comparing auto-correlation of a single channel (channel 1 located at 229 m) (black line) and  $q(t)$  (red line). When a single channel is used, it can be observed that sidelobes are generated after a certain zone (blue box area in Fig. 9). However, when all channels are used, the sidelobes are reduced and the function is closer to the delta function, unlike in the case of using a single channel.

Time reversal processing is a technique that allows signal reconstruction from matched filtering of a received signal and a channel impulse response, and before the

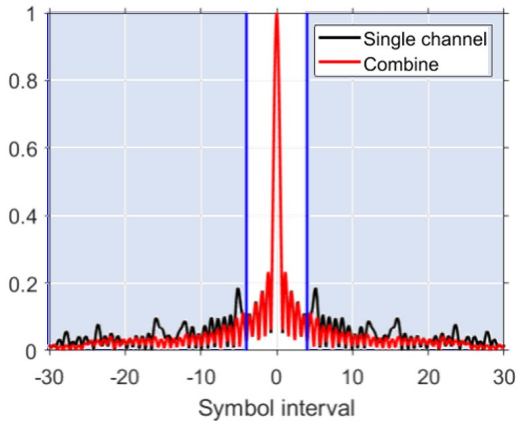


Fig. 9. (Color available online) Auto-correlation of channel impulse response at 179-m depth (black line) and  $q(t)$  calculated from the probe signal (red line).

performance analysis of communication signals, the signal reconstruction performance is examined using probe signals.

$$\tilde{S}(\omega) = \mathbf{R}(\omega)\mathbf{H}^H(\omega) = \sum_{i=1}^N R_i(\omega)H_i^*(\omega). \quad (4)$$

Eq. (4) represents the time reversal processing technique;<sup>[26]</sup>  $\mathbf{R}(\omega)$  and  $\mathbf{H}(\omega)$  denote the spectrum of the received signals and transfer function in all channels, respectively;  $(\cdot)^H$  represents the Hermitian matrix, which is a matrix equal to its conjugate transpose;  $i$  is the channel number;  $\tilde{S}(\omega)$  is the final result of time reversal processing, and the reconstructed signal can be obtained by performing the inverse Fourier transform after performing calculations for all frequency components. Fig. 10 shows the results of applying the time reversal processing to the probe signals. Although some distortion is apparent, the overall shape is similar to the probe signal with the application of a 0.5 s-Hanning window. The slight distortion that can be observed in Fig. 10 is presumed to occur because  $q(t)$  is not a perfect delta function, as in the case of Fig. 9. To quantitatively evaluate the degree of reconstruction, the maximum value of the cross-correlation coefficient between the transmitted probe signal and the probe signal reconstructed through time-reversal processing was cal-

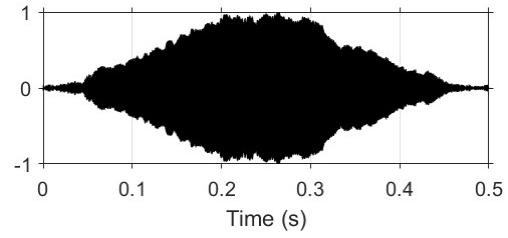


Fig. 10. Probe signal reconstructed using time reversal processing.

culated using Eq.(5). The maximum cross-correlation coefficient between the result of Fig. 10 and the transmitted signal was approximately 99%, confirming that the proposed time reversal processing has good performance.

$$CCC = \max \left( \frac{\int_{-\infty}^{\infty} S(\omega)\tilde{S}^*(\omega)e^{-i\omega t}d\omega}{\int_{-\infty}^{\infty} |S(\omega)|^2d\omega \int_{-\infty}^{\infty} |\tilde{S}(\omega)|^2d\omega} \right). \quad (5)$$

From the result of Figs. 9 and 10, successful signal reconstruction can be confirmed, serving as a metric that allows prediction of the successful demodulation of communication signals.

## 4.2 Results of communication performance analysis

As can be observed from the results obtained using the probe signal as in the previous section, time reversal processing, which is known to derive an optimal solution, was used for the communication performance analysis. Before time reversal processing, Doppler estimation as described in Section 3.2 was performed for each channel and the Doppler effect is compensated in the received signal. Because time reversal processing has the same principle as the equalizer, in theory, it can also be referred to as a self-equalizer.<sup>[29]</sup> However, in practice, residual Inter-Symbol Interference (ISI) remains even after time-reversal processing. To eliminate this, the single-channel decision feedback equalizer is mainly applied, and the combination of time reversal processing and equalizer is

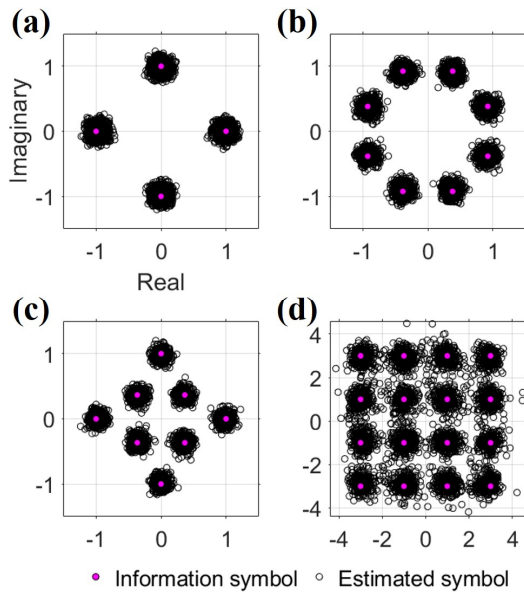


Fig. 11. (Color available online) Scatter plots of higher-order modulation based on time reversal processing with decision feedback equalizer: (a) QPSK, (b) 8PSK, (c) 8QAM, and (d) 16QAM.

known as the optimal solution<sup>[25,26]</sup>. In this study, after time reversal processing, the decision feedback equalizer was applied using the training symbols located in the front part of the payloads to analyze the communication performance. In particular, an adaptive algorithm of recursive least squares with the forgetting factor of 0.99 was employed, and the numbers of feed forward and feedback filter taps were designed to be 20 and 10, respectively.

Fig. 11 displays scatter plots of the results of applying the time reversal processing and decision feedback equalizer to two types of PSK modulation and two types of QAM. Figs. 11(a) and 11(b) show the results of the QPSK and 8PSK modulation types, respectively, and Figs. 11(c) and 11(d) present the results of the 8QAM and 16QAM types, respectively. In the case of PSK modulation, an error symbol does not appear, and it can be observed that the estimated symbols form around the information symbol. This indicates that the output SNR, which expresses how widely the estimated symbols are distributed from the information symbols, of these signals is large.<sup>[28]</sup> Conversely, in the case of 8QAM among the QAM types, there was no error symbol, but for 16QAM, 403 bit errors

Table 1. Bit Error Rate (BER) and output SNR according to the modulation type.

Modulation	BER	Output SNR
QPSK	0/10400 (0 %)	18.9 dB
8PSK	0/15600 (0 %)	18.9 dB
8QAM	0/15600 (0 %)	18.5 dB
16QAM	403/20800 (1.94 %)	12.3 dB

occurred out of 20,800 bits. Although both 8PSK and 8QAM use three bits per symbol, the difference between the two types of modulation is that 8QAM includes amplitude modulation in addition to phase modulation. The amplitude modulation is ultimately determined by the influence of the background noise level. Because ACUA-EX20 is a favorable environment with an SNR of 10 dB or more, the performances of the two modulation schemes were similar. In the case of 16QAM, which is more sensitive to noise because the Euclidean distance is shorter than that of 8QAM, some bit errors occur. However, because it shows a low Bit Error Rate (BER) of approximately 2 %, it can be inferred that 16QAM, which is a challenging higher-order modulation, was also successfully demodulated. Table 1 summarizes the results of the BER and output SNR for each modulation type. From all the results, the feasibility of higher-order modulation to increase the data rate was verified in long-range underwater acoustic communication.

For approximate comparative analysis on the level of the signals designed in this study, Fig. 12 depicts a comparison with the results of overseas studies in a similar environment, and Table 2 outlines the signal design specifications and transmission range in this study and existing overseas studies. A similar deep-water environment was defined in this study with a range of less than 50 km and a water depth of 1,000 m or more. The black dashed line in Fig. 12 indicates the metric (range-rate product) proposed in Reference [2], and the yellow star-shaped values denote the specifications of the signals used in this study. To show the results of overseas studies, BPSK, QPSK, and 8PSK modulation schemes are indicated in red, blue, and green, respectively, and the results of

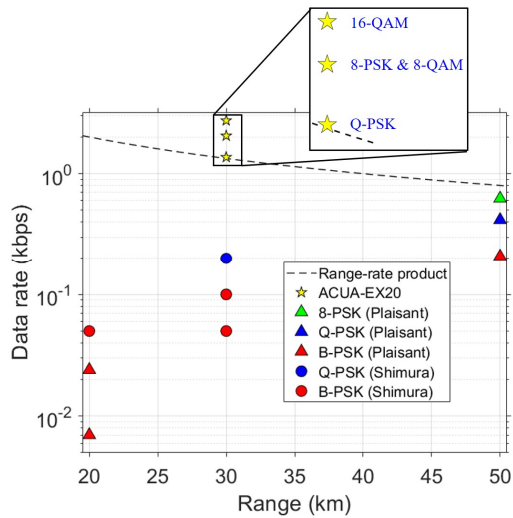


Fig. 12. (Color available online) Comparison of performance for ACUA-EX20 with that in studies with a similar environment (range of less than 50 km and deep sea with a depth of more than 1,000 m)

Table 2. Range and specification in studies shown in Fig. 12.

Authors	Range (km)	Frequency (Hz)		Modulation	bps (bits/s)	Spectral efficiency (bits/s/Hz)
		Carrier	Bandwidth			
ACUA-EX20	23	2,560	1,024	QPSK / 8PSK / 8QAM / 16QAM	1,365 / 2,048 / 2,048 / 2,731	1.33 / 2 / 2 / 2.67
Shimura <i>et al.</i>	20 / 30 / 40	500	100	BPSK	100	1
	30					
Plaisant <i>et al.</i>	50	1,700	400	BPSK / QPSK / 8PSK	208 / 417 / 625	0.52 / 1.04 / 1.56
	20	1,666	520	BPSK	7 / 24	0.01 / 0.05

Shimura and Plaisant are indicated by circles and triangles, respectively. When compared with the results of overseas studies in similar environments, the data rates of the signals designed in this study were high. In addition, the enlarged figure in Fig. 12 shows that the data rate exceeded the metric values presented in Reference [2]. However, because the results in Fig. 12 do not include the sea environment and system specifications, such as fre-

quency, bandwidth, source level, and array arrangement, apart from the signal design, there are limitations in terms of comparison between the different results. Therefore, only the confirmation on the approximate level is possible at this stage, to improve precision, comparisons should be made considering the sea environment and system specifications.

## V. Conclusions

In long-range underwater acoustic communication, the data rate is reduced because of the narrow bandwidth. To increase the data rate under the condition of limited bandwidth, in this study, we conducted analysis of deep-water long-range communication using higher-order modulation, the performance results of which are presented herein, verifying the feasibility of higher-order modulation in the long-range communication environment in deep water. In addition, we designed two types of PSK and QAM (QPSK and 8PSK, 8QAM and 16QAM) as signals of high-order modulation and used for transmission. The range between the source and receiver was 23 km, and the source was towed in the east direction at the speed of 3 kn. For communication performance analysis, a combination of time reversal processing and a single channel decision feedback equalizer, known as optimal solutions, was employed. Before the application of time reversal processing, a Doppler effect caused by towing the source have to be compensated. Through this process, the BER of 0 % and an output SNR of 18 dB or more were obtained in the modulation schemes except for 16QAM; the highest order modulation; in this case, a BER of less than 2 % and an output SNR of more than 12 dB were obtained. From the above results, the feasibility of higher-order modulation was experimentally verified for increasing data rate in a long-range environment.

## Acknowledgement

This work was supported by the Agency for Defense

Development, South Korea, under Grant UD200010DD and Low frequency Underwater Research Laboratory.

## References

1. Y. Zhou, A. Song, and F. Tong, "Underwater acoustic channel characteristics and communication performance at 85 kHz," *J. Acoust. Soc. Am.* **142**, EL350-EL355 (2017).
2. D. B. Kilfoyle and A. B. Baggeroer, "The state of the art in underwater acoustic telemetry," *IEEE J. Ocean Eng.* **25**, 4-27 (2000).
3. Y. Kida, M. Deguchi, and T. Shimura, "Experimental results for a high-rate underwater acoustic communication in deep sea for a manned submersible SHINKAI 6500," *J. Marine Acoust. Soc. Jpn.* **43**, 197-203 (2018).
4. M. Stojanovic, J. Catipovic, and J. G. Proakis, *Acoustic Signal Processing for Ocean Exploration* (Springer, Dordrecht, 1993), pp.607-612.
5. M. Stojanovic, J. Catipovic, J. G. Proakis, "Adaptive multichannel combining and equalization for underwater acoustic communications," *J. Acoust. Soc. Am.* **94**, 1621-1631 (1993).
6. A. Plaisant, "Long range acoustic communications," *Proc. IEEE OCEANS'98 Conference*, 1 (1998).
7. T. Shimura, Y. Watanabe, H. Ochi, and T. Hattori, "Basic at-sea experiment for long horizontal time-reversal communication in deep ocean," *Proc. Acoustics '08*, 10375-10380 (2008).
8. H. C. Song, W. A. Kuperman, and W. S. Hodgkiss, "Basin-scale time reversal communications," *J. Acoust. Soc. Am.* **125**, 212-217 (2009).
9. H. C. Song and M. Dzieciuch, "Feasibility of global-scale synthetic aperture communications," *J. Acoust. Soc. Am.* **125**, 8-10 (2009).
10. T. Shimura, H. Ochi, Y. Watanabe, and T. Hatton, "Experiment results of time-reversal communication at the range of 300 km," *Jpn. J. Appl. Phys.* **49**, 07HG11 (2010).
11. H. C. Song, S. Cho, T. Kang, W. S. Hodgkiss, and J. R. Preston, "Long-range acoustic communication in deep water using a towed array," *J. Acoust. Soc. Am.* **129**, EL71-EL75 (2011).
12. T. Shimura, H. Ochi, and Y. Watanabe, "Time - reversal communication in deep ocean - results of recent experiments," *Proc. 2011 IEEE Symposium on Underwater Technology and Workshop on Scientific Use of Submarine Cables and Related Technologies*, 1-5 (2011).
13. H. C. Song, "Acoustic communication in deep water exploiting multiple beams with a horizontal array," *J. Acoust. Soc. Am.* **132**, EL81-EL87 (2012).
14. H. C. Song and W. S. Hodgkiss, "Diversity combining for long-range acoustic communication in deep water," *J. Acoust. Soc. Am.* **132**, EL68-EL73 (2012).
15. T. Kang, H. C. Song, and W. S. Hodgkiss,, "Long-range multi-carrier acoustic communication in deep water using a towed horizontal array," *J. Acoust. Soc. Am.* **131**, 4665-4671 (2012).
16. T. Shimura, Y. Watanabe, H. Ochi, and H. C. Song, "Long-range time reversal communication in deep water : Experimental results," *J. Acoust. Soc. Am.* **132**, EL49-EL53 (2012).
17. T. Shimura, H. Ochi, and H. C. Song, "Experimental demonstration of multiuser communication in deep water using time reversal," *J. Acoust. Soc. Am.* **134**, 3223-3229 (2013).
18. Z. Liu, K. Yoo, T. C. Yang, S. E. Cho, H. C. Song, and D. E. Ensberg "Long-range double-differentially coded spread-spectrum acoustic communications with a towed array," *IEEE J. Ocean Eng.* **39**, 482-490 (2014).
19. T. Shimura, Y. Kida, M. Deguchi, Y. Watanabe, and H. Ochi, "At-sea experiment of adaptive time-reversal multiuser communication in the deep ocean," *Jpn. J. Appl. Phys.* **54**, 07HG02 (2015).
20. J. Lee, H. Lee, K. Kim, and W. Kim, "Sea trial results of long range underwater acoustic communication based on frequency modulation in the East Sea" (in Korean), *J. Acoust. Soc. Kr.* **38**, 371-377 (2019).
21. H. S. Kim, S. H. Kim, J. W. Choi, and H. S. Bae,, "Bidirectional equalization based on error propagation detection in long-range underwater acoustic communication," *Jpn. J. Appl. Phys.* **58**, SGGF01 (2019).
22. H. Park, D. Kim, J. S. Kim, J. Hahn, and J. Park, "Performance improvement of long-range underwater acoustic communication in deep water using spatio-temporal diversity" (in Korean), *J. Acoust. Soc. Kr.* **38**, 587-592 (2019).
23. D. Kim, H. Park, J. S. Kim, J. Hahn, and J. Park, "Performance analysis of underwater acoustic communication based on beam diversity in deep water" (in Korean), *J. Acoust. Soc. Kr.* **38**, 678-686 (2019).
24. G. F. Edelmann, T. Akai, W. S. Hodgkiss, S. Kim, W. A. Kuperman, and H. C. Song, "An initial demonstration of underwater acoustic communication using time reversal," *IEEE J. Ocean Eng.* **27**, 602-609 (2002).
25. G. F. Edelmann, H. C. Song, S. Kim, W. S. Hodgkiss, W. A. Kuperman, and T. Akai, "Underwater acoustic communication using time reversal," *IEEE J. Ocean Eng.* **30**, 852-864 (2005).
26. H. C. Song, W. S. Hodgkiss, W. A. Kuperman, M. Stevenson, and T. Akai, "Improvement of time-reversal communications using adaptive channel equalizers," *IEEE J. Ocean Eng.* **31**, 487-496 (2006).

27. M. I. Skolnik, *Introduction to Radar Systems* (McGraw-Hill, Boston, 2001), pp. 411-420.
28. H. C. Song, W. S. Hodgkiss, W. A. Kuperman, W. J. Higley, K. Raghukumar, T. Akai, and M. Stevenson, "Spatial diversity in passive time reversal communication," *J. Acoust. Soc. Am.* **120**, 2067-2076 (2006).
29. H. C. Song, "An overview of underwater time-reversal communication," *IEEE J. Ocean Eng.* **41**, 644-655 (2016).

## Profile

### ▶ Donghyeon Kim (김동현)



He received the B.S. and M. S. degrees in ocean engineering from Korea Maritime and Ocean University, Busan, South Korea, in 2014 and 2016, respectively. He is currently working toward the Ph.D. degree in convergence study on the ocean science and technology at Korea Maritime and Ocean University, Busan, South Korea. His research interests include time-reversed acoustics, underwater acoustic communications and signal processing.

### ▶ J. S. Kim (김재수)



He received the B.S. degree in naval architecture from Seoul National University, Seoul, South Korea, in 1981, the M.S. degree in department of coastal and oceanographic engineering from University of Florida, Gainesville, in 1984, and the Ph.D. degree in ocean engineering from Massachusetts Institute of Technology, Cambridge, in 1989. He has been working for ocean engineering in Korea Maritime and Ocean University as a professor since 1991. From 1990 to 1991, he was with the Agency for Defense Development, Changwon, South Korea. In 1999-2001 and 2009-2010, he was a visiting scientist at the Scripps Inst. of Oceanography (SIO), University of California, San Diego, CA, USA. His research interests include time-reversed acoustics, wave propagation physics, and signal processing.

### ▶ Joo Young Hahn (한주영)



He received the B.S., M. S., Ph. D. degrees in earth and marine sciences from Hanyang University, Ansan, South Korea, in 1997, 2000, and 2004, respectively. Since 2005, he has been with the Agency for Defense Development, Changwon, South Korea, where he is currently a Senior Research Scientist. His research interests include channel modeling and source localization.